JPE 18-1-5

https://doi.org/10.6113/JPE.2018.18.1.45
ISSN(Print): 1598-2092 / ISSN(Online): 2093-4718

Optimized Operation of Dual-Active-Bridge DC-DC Converters in the Soft-Switching Area with Triple-Phase-Shift Control at Light Loads

Li Jiang*, Yao Sun*, Mei Su*, Hui Wang*, and Hanbing Dan†

*,†School of Information Science and Engineering, Central South University, Changsha, China

Abstract

It is usually difficult for dual-active-bridge (DAB) dc-dc converters to operate efficiently at light loads. This paper presents an in-depth analysis of a DAB with triple-phase-shift (TPS) control under the light load condition to overcome this problem. A kind of operating mode which is suitable for light load operation is analyzed in this paper. First, an analysis of the zero-voltage-switching (ZVS) constraints for the DAB converter has been carried out and a reasonable dead-band setting method has been proposed. Secondly, the basic operating characteristics of the converter are analyzed. Third, under the condition of satisfying the ZVS constraints, both the reactive power and the root mean square (RMS) value of the current are simultaneously minimized and a particle swarm optimization (PSO) algorithm is employed to analyze and solve this optimization problem. Lastly, both simulations and experiments are carried out to verify the effectiveness of the proposed method. The experimental results show that the converter can effectively achieve ZVS and improved efficiency.

Key words: Dead-band, Dual-active-bridge (DAB), Particle swarm optimization (PSO), Reactive power, RMS value of current, Soft-switching, Triple-phase- shift (TPS)

I. INTRODUCTION

In recent years, dual-active-bridge (DAB) dc-dc converters have received more and more attention. The DAB dc-dc converter was originally introduced in the 90's [1]. Due to its advantages in terms of high-power density, zero voltage switching (ZVS), electrical isolation, bidirectional power transmission and modularity, it has gained a lot of popularity and been widely used in distributed power generation systems, hybrid electric vehicles (HEVs), microgrids and battery energy storage systems [2]-[8].

Phase-shift control schemes including single-phase-shift (SPS) control, dual-phase-shift (DPS) control, extended-phase-shift (EPS) control and triple-phase-shift (TPS) control, have been widely applied in DAB converters. In the SPS control, only the phase-shift angle can be controlled. If the voltages on both sides of the transformers do not match, the current stresses are high. In addition, it is hard to realize soft-switching [9], [16]. In the DPS control, the cross-connected switch pairs in both of the full bridges are switched with the inner phase-shift angle, and the two inner phase-shift angles are same [10], [11]. In the EPS control, the cross-connected switch pairs in one full bridge are switched in turn, while the switch pairs in the other full bridge are switched with the inner phase-shift angle [7]. Both the DPS and EPS controls have an external phase-shift angle between the two full-bridges. To further improve both the converter performance and the flexibility of the control, the TPS control was proposed in [12], [13]. In the TPS control, the inner phase-shift angle in both of the full bridges may be unequal. An analysis of the phase-shift control shows that all of the other phase-shift controls are only special cases of the TPS control.

It is important for DAB converters to works in optimized operation modes. Minimum current stress switching schemes for DAB converters with the TPS control and the corresponding control method are proposed in [14], [15]. In [16], the characteristics of the DAB converter are analyzed in

Manuscript received May 10, 2017; accepted Oct. 12, 2017
Recommended for publication by Associate Editor Il-Oun Lee.
†Corresponding Author: daniel698@sina.cn
Tel: +86-15200815824, Central South University
*School of Information Science and Engineering, Central South University, China

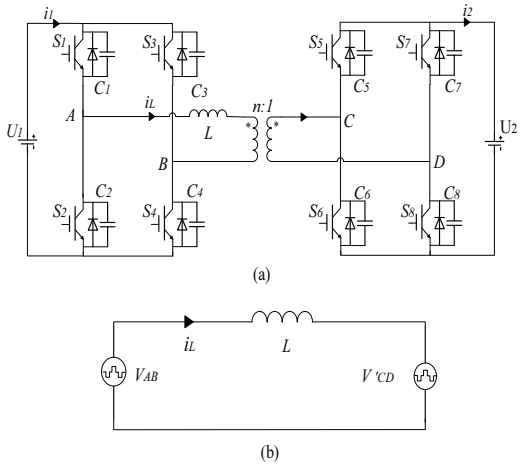

Fig. 1. DAB: (a) Schematic; (b) equivalent circuit.

detail with the EPS control and the TPS control. In addition, the minimum RMS values of the inductance current are chosen as optimization objectives. In order to improve efficiency, a strategy for minimizing the reactive power of the DAB with the DPS control was also proposed in [10] and [17]. The above optimization strategies are essentially the optimization and control of the inductor current. Some studies directly analyze the losses of the converter. An optimal modulation scheme with minimum conduction and copper losses is presented for the DAB with the TPS control in [13]. Similarly, on the basis of loss models, an efficiency-optimized switching strategy and the corresponding control of the converter with the DPS control are proposed in [18].

An analysis of soft-switching is always accompanied by an analysis of dead-band operation. An inappropriate dead-band degrades the performance of converters through voltage polarity reversal, voltage sag and phase drift [19]. To better understand the optimum dead-band and its main influencing factors, a double-pulse test was carried out to characterize the switching behavior, and an adaptive dead-band control scheme was proposed in [20]. The key to realizing soft-switching is to analyze and control the inductor current in the dead-band [21], [22]. In [15], the commutations in the dead-band are analyzed, and then the soft-switching constraints are obtained. These constraints are not strictly a prerequisite for converter optimization.

In this paper, the resonances in all of the dead-bands are analyzed in detail. At light loads, the converter current stress is very small and the effect of reactive power on efficiency is more significant [17]. In addition, the RMS value of the current is the main cause of copper and conduction losses. Thus, the optimization objectives in this paper include minimizing both the reactive power and the RMS value of the inductor current. The other parts of this paper are organized as follows. In section II, a detailed analysis of the ZVS constraints has been carried out and a reasonable dead-band setting method has been proposed. Then, the basic operating

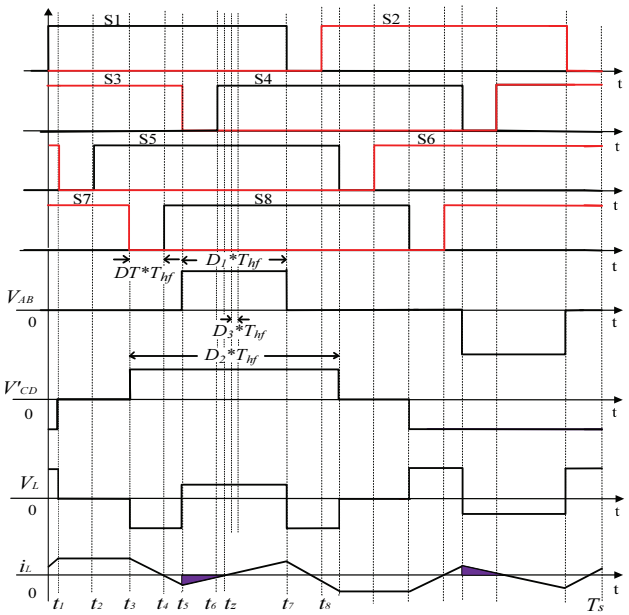

Fig. 2. Waveforms of a DAB with TPS control in the case of $-D_1+D_2-2D_3 \geq 0$.

characteristics of the converter at light loads are analyzed. In Section III, an optimized modulation scheme is proposed under the condition of the ZVS constraints. PSO is used to analyze and solve this optimization problem to get the three control parameters of the TPS control. In Section IV, both simulation and experimental results are illustrated. In the last section, some conclusions are given.

II. TPS Control Theory and an Analysis of the Light Load Operating Mode

The circuit topology of a DAB is shown in Fig. 1, where U_1 and U_2 are the DC voltage on both sides of the converter, L is the sum of the transformer leakage inductor and the auxiliary inductor. In the TPS control scheme for the DAB, the converter works in six operating modes depending on the different values of phase-shift angles when power is transmitted forward [16].

A. TPS Control Theory

The related waveforms of a converter with TPS control at a light-load are shown in Fig. 2, where the dead-band is magnified, V_{AB} and V'_{CD} are the equivalent ac output voltages of the two full bridges on U_1 side, T_{hf} represents half of the switching period, and i_L is the current through L. D_1 is the ratio of the high level time of V_{AB} to T_{hf}(D_1=(t_7-t_5)/T_{hf}), and D_2 is defined in the same way. The ratio of the phase difference between V_{AB} and V'_{CD} to π is defined as the duty ratio D_3. When the phase of V_{AB} is ahead of V'_{CD}, D_3 is positive, while D_3 is negative. The ratio of the dead-band to T_{hf} is DT. D_1 and D_2 are controlled by the inner phase-shift

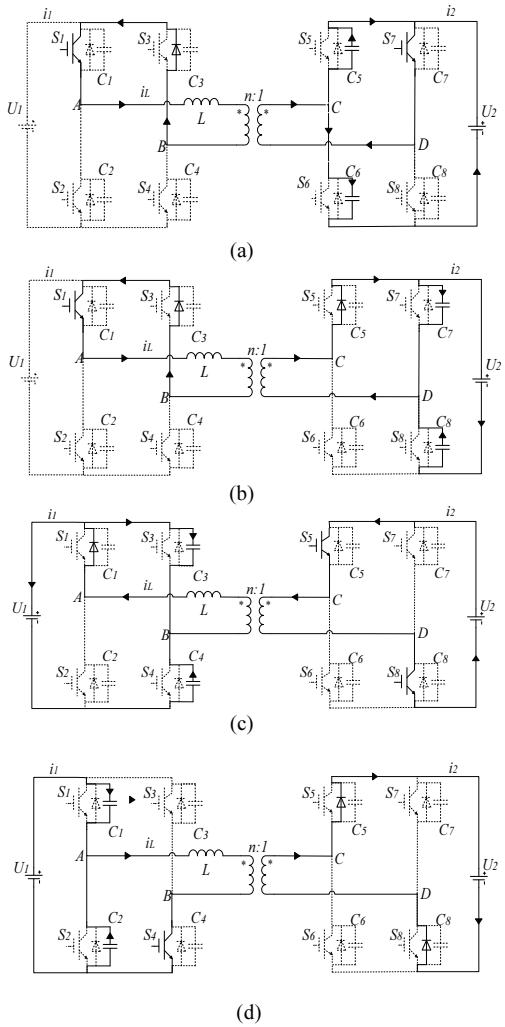

Fig. 3. Circuit state of a DAB in the dead-band: (a) dead-band of [t_1, t_2]; (b) dead-band of [t_3, t_4]; (c) dead-band of [t_5, t_6]; (d) dead-band of [t_7, t_8].

angles of both of the full bridges, and the D_3 is controlled by the outer phase-shift angle between the two full bridges. n is the turns ratio of the transformer, and the voltage conversion ratio k is define as $k=nU_2/U_1$. Only the case of $D_3>0$ and $k\leq 1$ is analyzed in this paper. However, other conditions could be analyzed similarly.

B. Analysis of Resonance in the Dead-band

The light-load operating mode is characterized by the rising edge of V'_{CD} from 0 to U_2 leading the rising edge of V_{AB} from 0 to U_1, and lagging the rising edge of V_{AB} from $-U_1$ to 0 [15], [16]. Thus, only this mode is analyzed in this section. To work in the light-load mode, the following constraint should be satisfied:

$$-D_1 + D_2 - 2D_3 \geq 0 \tag{1}$$

Since the waveforms of the DAB are anti-symmetric at every half-switching cycle, the resonance analysis is only carried out in the first half of the cycle.

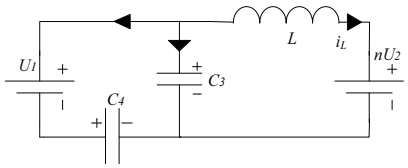

Fig. 4. Equivalent circuit of a DAB in the dead-band of [t_5, t_6].

During [t_5, t_6], which is a dead-band, S_1, S_5 and S_8 are on, S_3 is turned off at $t=t_5$ at an approximate ZVS because the voltage of C_3 cannot mutate. In the interval, the inductor L resonates with C_3 and C_4 to complete the process of discharging C_4 and charging C_3 as shown in Fig. 3(c). Since $i_L(t) \leq 0$ in this interval, if the anti-parallel diode of S_4 begins to conduct after the voltage of C_4 is clamped to zero, S_4 could be turned on at the ZVS condition. The equivalent circuit in this process is shown in Fig. 4. The differential equations of the circuit in Fig. 4 are derived as follows:

$$\begin{cases} -i_L(t-t_5) = C_3 \dfrac{du_{C_3}(t-t_5)}{dt} + C_4 \dfrac{du_{C_4}(t-t_5)}{dt} \\ U_1 + u_{C_4}(t-t_5) = L\dfrac{di_L(t-t_5)}{dt} + nU_2 \end{cases} \tag{2}$$

With the initial conditions: $u_{C4}(0)=-U_1$ and $i_L(0)=i_L(t_5)$. The solutions of (2) are expressed as follows:

$$\begin{cases} u_{C_4}(t-t_5) = -U_{m4}\sin(\omega_4(t-t_5)+\alpha_4) + nU_2 - U_1 \\ i_L(t-t_5) = i_L(t_5)\cos\omega_4(t-t_5) - \dfrac{nU_2}{Z_L}\sin\omega_4(t-t_5) \end{cases} \tag{3}$$

where, $C_{L1}=C_3+C_4$, $\omega_4=1/\sqrt{LC_{L1}}$, $Z_{L1}=\sqrt{L/C_{L1}}$,

$tan\alpha_4 = nU_2/(Z_{L1}i_L(t_5))$, $U_{m4}=\sqrt{[Z_{L1}i_L(t_5)]^2+(nU_2)^2}$.

Similarly, according to Fig. 3(a), (b) and (d), the related variables in the dead-bands [t_1, t_2], [t_3, t_4] and [t_7, t_8] are expressed as follows:

$$\begin{cases} u_{C_5}(t-t_1) = U_{m5}\sin(\omega_5(t-t_1)-\alpha_5) \\ i_L(t-t_1) = i_L(t_1)\cos\omega_5(t-t_1) + \dfrac{C_{R1}U_2}{\sqrt{LC_{R1}}}\sin\omega_5(t-t_1) \end{cases} \tag{4}$$

where, $C_{R1}=C_5+C_6$, $\omega_5=n/\sqrt{LC_{R1}}$, $Z_{R1}=\sqrt{L/C_{R1}}$,

$tan\alpha_5 = U_2/(Z_{R1}i_L(t_1))$, $U_{m5}=\sqrt{[Z_{R1}i_L(t_1)]^2+U_2^2}$.

$$\begin{cases} u_{C_8}(t-t_3) = U_{m8}\sin\omega_8(t-t_3) - U_2 \\ i_L(t-t_3) = i_L(t_3)\cos\omega_8(t-t_3) \end{cases} \tag{5}$$

where, $C_{R2}=C_7+C_8$, $\omega_8=n/\sqrt{LC_{R2}}$, $Z_{R2}=\sqrt{L/C_{R2}}$,

$U_{m8}=Z_{R2}i_L(t_3)$.

$$\begin{cases} u_{C_2}(t-t_7) = U_{m2}\sin(\omega_2(t-t_7)+\alpha_2) - nU_2 \\ i_L(t-t_7) = i_L(t_7)\cos\omega_2 t - \dfrac{nU_2-U_1}{Z_{L2}}\sin\omega_2(t-t_7) \end{cases} \tag{6}$$

where, $C_{L2}=C_1+C_2$, $\omega_2=1/\sqrt{LC_{L2}}$, $Z_{L2}=\sqrt{L/C_{L2}}$,

$tan\alpha_2 = nU_2/(Z_L i_L(t_7))$, $U_{m2}=\sqrt{[Z_{L2}i_L(t_7)]^2+(nU_2-U_1)^2}$.

TABLE I
VALUE OF EACH TIME POINT

t_1	$\frac{T_s}{2}(-\frac{D_1}{2}+\frac{D_2}{2}+D_3-DT)$
t_2	$\frac{T_s}{2}(-\frac{D_1}{2}+\frac{D_2}{2}+D_3)$
t_3	$\frac{T_s}{2}(1-\frac{D_1}{2}-\frac{D_2}{2}+D_3-DT)$
t_4	$\frac{T_s}{2}(1-\frac{D_1}{2}-\frac{D_2}{2}+D_3)$
t_5	$\frac{T_s}{2}(1-D_1-DT)$
t_6	$\frac{T_s}{2}(1-D_1)$
t_7	$\frac{T_s}{2}(1-DT)$

To achieve ZVS, the dead-band must be greater than the time in which the voltage of the capacitor connected in parallel across the switch drops to zero since the resonance occurs. From (3), (4), (5) and (6), it is know that the shortest time of any point to zero is not greater than a quarter of the resonant cycle. Thus, the dead-band can be set to a quarter of the resonant cycle. This can be based on the required dead-band to set the parameters of the inductor and the parallel capacitor. The resonant cycle is adjusted to four times the dead-band. This condition can be derived as follows:

$$\begin{cases} DTT_S/2=1/(4f) \\ C_1=C_2=C_3=C_4 \\ C_5=C_6=C_7=C_8 \\ n^2C_{L1}=C_{R1} \\ 2\pi f=\omega_4=\omega_5 \end{cases} \tag{7}$$

where f is the resonant frequency.

C. Light-load Operating Characteristics

The effect of resonance on the output voltages of an H-bridge inverter can be neglected when the switching frequency is relatively low. According to the equivalent circuit of the DAB converter in Fig. 1(b) and Fig. 2, the steady-state current through inductor L can be expressed in (8), and times $t_1, t_2, \cdots t_8$ are listed in Table I.

$$i_L(t)=\begin{cases} \frac{kU_1}{L}t+\frac{U_1}{4Lf_s}\left[(k-1)D_1-2kD_3+2kDT\right] & (0\le t\le t_1) \\ \frac{U_1}{4Lf_s}(-D_1+kD_2) & (t_1\le t\le t_3) \\ -\frac{kU_1}{L}t+\frac{U_1}{4Lf_s}\left[2k-(k+1)D_1+2kD_3-2kDT\right] & (t_3\le t\le t_5) \\ \frac{(1-k)U_1}{L}t+\frac{U_1}{4Lf_s}\left[\begin{matrix}2k-2+(1-k)D_1+2kD_3 \\ +(2-2k)DT\end{matrix}\right] & (t_5\le t\le t_7) \\ -\frac{kU_1}{L}t+\frac{U_1}{4Lf_s}\left[2k+(1-k)D_1+2kD_3-2kDT\right] & (t_7\le t\le \frac{T_s}{2}) \end{cases} \tag{8}$$

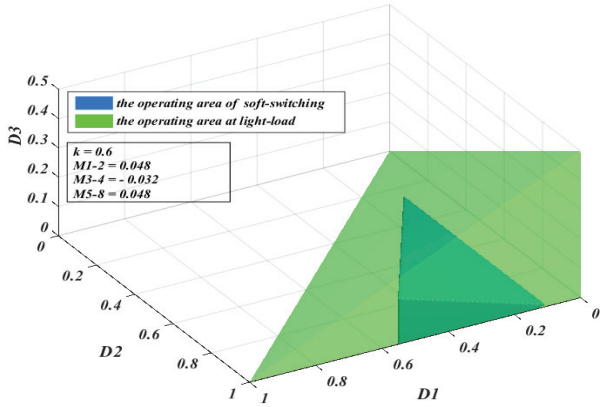

Fig. 5. Soft-switching area of a DAB with TPS control at a light load.

from Fig. 2, the average transmission power can be expressed as follows:

$$P=U_1\frac{1}{T_s/2}\int_{t_5}^{t_7}i_L(t)\,dt \tag{9}$$

According to Table I, (8) and (9), the expression of the normalized transmission power can be derived as follows:

$$\overline{P}=\frac{P}{P_{base}}=4kD_1D_3 \tag{10}$$

where P_{base} is defined as follows:

$$P_{base}=\frac{U_1^2}{8Lf_s} \tag{11}$$

According to (10), transmission power is a function of D_1 and D_3 in this operating mode.

D. Soft-switching Constrains

According to the previous resonance analysis, two constraints for ZVS must be satisfied. One is that the direction of the inductor current needs to suit the commutation in the dead-band, and this current direction does not change within this dead-band. The other is that the inductor current must be large enough to complete the charging and discharging processes of the capacitors. According to the same switching characteristic of the switches in the same bridge leg, to ensure that S_1 and S_2 can be switched under ZVS, the inductor current must be greater than zero during the whole dead-band [t_7, t_8]. This condition can be formulated as follows:

$$i_L(t_8)\ge 0 \tag{12}$$

According to (8) the condition (12) is rewritten as:

$$(1-k)D_1+2kD_3\ge 2kDT \tag{13}$$

According to (6), to ensure that the voltage across C_2 can resonate to zero, the condition in (14) must be satisfied.

$$U_{m2}\ge nU_2 \tag{14}$$

By combining the value of U_{m2} and (8), equation (14) can be rewritten as follows:

$$(1-k)D_1+2kD_3\ge 4f_s\sqrt{L(C_1+C_2)|2k-1|} \tag{15}$$

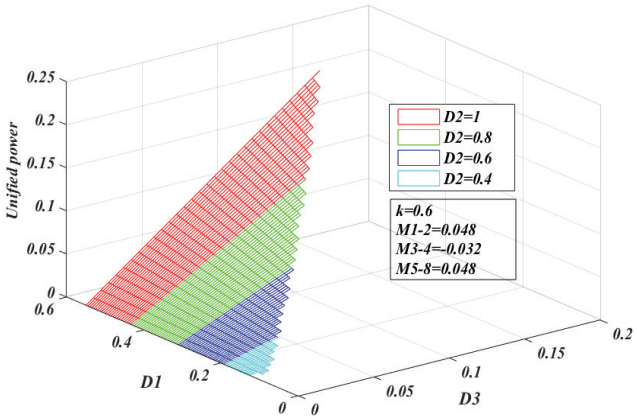

Fig. 6. Unified power $\overline{P}$ with D_1, D_2 and D_3 in the soft-switching area.

Similarly, to ensure that the switches S_3 , S_4 , S_5 , S_6 , S_7 and S_8 are switched under ZVS, the following conditions must be met.

$$\begin{cases}(k-1)D_1+2kD_3 \le (2k-2)DT \\ (k-1)D_1+2kD_3 \le -4f_s\sqrt{L(C_3+C_4)|2k-1|}\end{cases} \tag{16}$$

$$-D_1+kD_2 \ge 0 \tag{17}$$

$$\begin{cases}-D_1+kD_2 \ge 2kDT \\ -D_1+kD_2 \ge 4f_s\dfrac{k}{n}\sqrt{L(C_7+C_8)}\end{cases} \tag{18}$$

For convenience, define the following parameters.

$$\begin{cases}M_{1-2}=\max\left[2kDT,4f_s\sqrt{L(C_1+C_2)|2k-1|}\right] \\ M_{3-4}=\min\left[(2k-2)DT,-4f_s\sqrt{L(C_3+C_4)|2k-1|}\right] \\ M_{5-8}=\max\left[0,2kDT,4f_s\dfrac{k}{n}\sqrt{L(C_7+C_8)}\right]\end{cases} \tag{19}$$

Then, the soft-switching constraints can be simplified as follows:

$$\begin{cases}(1-k)D_1+2kD_3 \ge M_{1-2} \\ (k-1)D_1+2kD_3 \le M_{3-4} \\ -D_1+kD_2 \ge M_{5-8}\end{cases} \tag{20}$$

According to (1) and (20), the operating area under the light-load condition and the soft-switching area are obtained as shown in Fig. 5. The soft-switching area is a fraction of the light-load operating area, and this area will be the domain of D_1, D_2, D_3 to optimize the operation of the converter. From (10) and (20), the power characteristic of the DAB in the soft-switching area is shown in Fig. 6. Clearly, to transfer a given power, there are infinite combinations of D_1, D_2, D_3 which meet the requirement of (20). Therefore, there exists a space for optimization to realize some optimal targets such as power losses minimization and reactive power minimization.

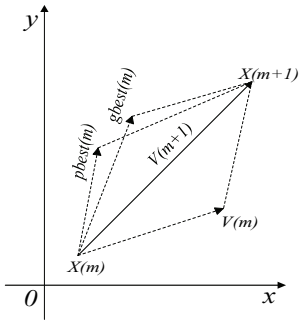

Fig. 7. Particle position update ($V_{pbest}(m)$ is the velocity based on $pbest(m)$, and $V_{gbest}(m)$ is based on $gbest(m)$).

III. Optimization Strategy Using Particle Swarm Optimization Algorithm

It is difficult for converters to operate efficiently especially at light loads. To maximize the efficiency of a DAB, reactive power and the RMS value of the inductor current should be minimized within the ZVS constraints.

A. Mathematical Model for Minimizing Reactive Power

For traditional buck, boost, or half-bridge converters, there is no reactive power because their power flow is always unidirectional within one switching cycle. However, in a DAB converter, the phase of the primary current is not always the same as the phase of the primary voltage. Therefore, there is a bidirectional transmission of power within one switching cycle. This means that a portion of the power is sent back from the load to the power supply, which results in lower efficiency. Referring to the definition of the reactive power of a converter with DPS control in [20], this is shown in the shaded area of Fig. 2.

From (8), the zero-crossing point of the current can be derived as follows:

$$t_z=\frac{1}{4(k-1)f_s}\left[2k-2+(1-k)D_1+2kD_3+(2-2k)DT\right] \tag{21}$$

The reactive power is defined as follows:

$$Q=-U_1\frac{1}{T_s/2}\int_{t_5}^{t_z} i_L(t)\,\mathrm{d}t \tag{22}$$

From (8), (21), (22) and Table I, the expression of the normalized reactive power is as follows:

$$\overline{Q}=\frac{Q}{P_{base}}=\frac{1}{2(1-k)}\left[(k-1)D_1+2kD_3\right]^2 \tag{23}$$

From (23), the reactive power is the function of D_1 and D_3. The optimization objective of the minimizing reactive power is formulated as follows:

$$\text{Minimize}\ \ \overline{Q} \tag{24}$$

B. Mathematical Model for Minimizing the Current RMS Value

Minimizing the RMS value of inductor current is an intuitive way to reduce power losses. The RMS value of the inductor current is expressed as follows:

$$i_{L(rms)} = \sqrt{\frac{\int_0^{T_s/2} i_L^2(t)\,dt}{T_s/2}} \tag{25}$$

From (8), (25) and Table I, the expression of the normalized RMS value is:

$$\bar{i}_{L(rms)} = \frac{i_{L(rms)}}{i_{base}} = \frac{2\sqrt{3}}{3}\left[\begin{matrix}(k-2)D_1^3 + 3D_1^2 + 3kD_1D_2^2 - 6kD_1D_2 \\ +12kD_1D_3^2 - 2k^2D_2^3 + 3k^2D_2^2\end{matrix}\right]^{1/2} \tag{26}$$

where i_{base} is defined as follows:

$$i_{base} = \frac{U_1}{8Lf_s} \tag{27}$$

Therefore, the optimization objective to minimize the RMS value of the inductor current is formulated as follows:

$$\text{Minimize} \quad \bar{i}_{L(rms)} \tag{28}$$

Based on the analysis above, to improve the efficiency of a DAB, a optimization problem of simultaneously minimizing the reactive power and minimizing the RMS value of the inductor current is formulated as follows:

$$\text{Minimize } [\bar{Q}, \bar{i}_{L(rms)}]' \tag{29}$$

$$s.t.\begin{cases} g_1 = D_1 + 2D_3 - D_2 \le 0 \\ g_2 = (k-1)D_1 - 2kD_3 + M_{1-2} \le 0 \\ g_3 = (k-1)D_1 + 2kD_3 - M_{3-4} \le 0 \\ g_4 = D_1 - kD_2 + M_{5-8} \le 0 \\ h_1 = 4kD_1D_3 - \bar{P} = 0 \\ 0 < D_1, D_2 \le 1 \\ 0 < D_3 \le 0.5 \end{cases} \tag{30}$$

from (29) and (30), since the objective functions and constraints are nonlinear, the traditional methods that depend on gradient information or the Lagrange multiplier theory are not very suitable for this problem. Thus, a particle swarm optimization (PSO) algorithm is used to analyze and solve these problems to get three optimal parameters of the TPS control.

In order to simplify the operation of PSO, the optimization problem can be simplified. First, the constraints in (30) can be transformed into an objective as follows:

$$\begin{aligned} f_0 = {} & \max(0, g_1) + \max(0, g_2) + \max(0, g_3) \\ & + \max(0, g_4) + h_1^2 \end{aligned} \tag{31}$$

Second, by adding weights to each of the optimization objectives, the multi-objective can be simplified to a single objective. The final optimization problem is formulated as follows:

$$\begin{cases} \text{Minimize } f = \lambda\bar{Q} + (1-\lambda)\overline{i_{L(rms)}} + \lambda_0 f_0 \\ 0 < D_1, D_2 \le 1 \\ 0 < D_3 \le 0.5 \\ 0 \le \lambda \le 1 \end{cases} \tag{32}$$

where λ is the weight of $\bar{Q}$, and λ_0 represents the penalty force for the violation of constraints. It is possible to get different optimization results by adjusting the value of λ, and a comparison of the optimization results can obtain the most suitable λ. The penalty force λ_0 need to be set so that it is large enough.

TABLE II
PARAMETERS OF THE DAB CONVERTER PROTOTYPE

DC voltage U_1	50 V
DC voltage U_2	10-15 V
Transformer turns ratio	2.5:1
Series inductor L	77.22 uH
Capacitor C_1, C_2, C_3, C_4	About 2.62 nF
Capacitor C_5, C_6, C_7, C_8	About 16.4 nF
Switching frequency f_s	20 KHz

C. Particle Swarm Optimization Algorithm

In the particle swarm optimization algorithm (PSO), each of the particles represents a possible solution. In the n-dimensional space, $X_i = (x_{i1}, x_{i2}, \ldots, x_{in})$ is the current position of the i-th particle, and $V_i = (v_{i1}, v_{i2}, \ldots, v_{in})$ is the current velocity. Let $f(x)$ be the minimization fitness function, while N is the number of particles. $pbest_i = (pbest_1, pbest_2, \ldots, pbest_n)$ is the best position that the i-th particle has experienced, and $gbest = (gbest_1, gbest_2, \ldots, gbest_n)$ is the best position that all of the particles have experienced. The velocity and position of each particle is updated by the following equations.

$$\begin{aligned} v_{ij}(m+1) = {} & \omega v_{ij}(m) + c_1 r_1 \left(pbest_{ij}(m) - x_{ij}(m)\right) \\ & + c_2 r_2 \left(gbest_{ij}(m) - x_{ij}(m)\right) \end{aligned} \tag{33}$$

$$x_{ij}(m+1) = x_{ij}(m) + v_{ij}(m+1) \tag{34}$$

where j denotes the j-th dimension in the n-dimensional space, m denotes the iteration of the particle swarm to the m-th generation, ω is the particle inertia, c_1 is the cognitive acceleration constant, c_2 is the social acceleration constant, and r_1 and r_2 are random numbers between 0 and 1. The scheme of the position update is illustrated in Fig. 7.

In the early stages of the iterations, the algorithm needs to have a strong global search capability to prevent prematurity. In the late stages of the iterations, a more detailed search is needed to speed up the convergence [23]. Use a time-varying inertia weight factor as follows:

$$\omega = (\omega_{\max} - \omega_{\min})\frac{M-m}{M} + \omega_{\min} \tag{35}$$

Similarly, the time-varying acceleration coefficient is proposed in [24]. It is defined as follows:

$$\begin{cases} c_1 = (c_{1\max} - c_{1\min})\dfrac{M-m}{M} + c_{1\min} \\ c_2 = (c_{2\max} - c_{2\min})\dfrac{m}{M} + c_{2\min} \end{cases} \tag{36}$$

In (35) and (36), ω_{max} is equal to 0.9, ω_{min} is equal to 0.4, c_{1max} and c_{2max} are equal to 2.5, c_{1min} and c_{2min} are equal to 0.5, and M and m are the maximum number and the current number of allowable iterations, respectively.

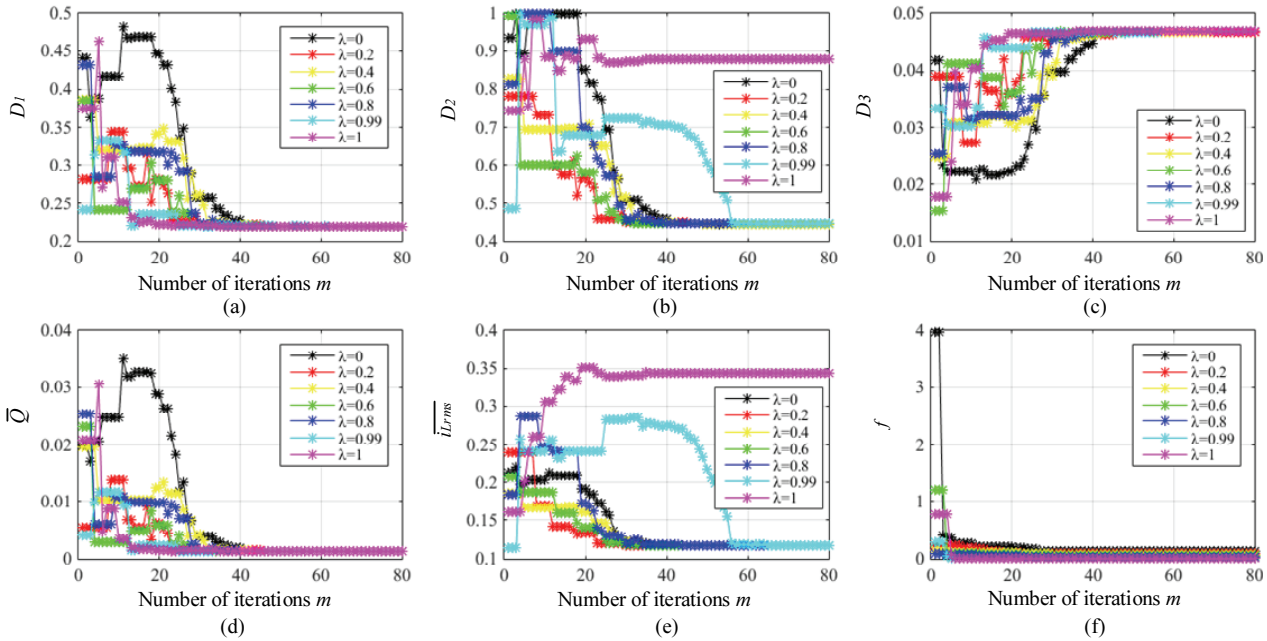

Fig. 8. Evolutionary process and optimal results of PSO at different weights λ when U_2 =12V and P = 5W: (a) D_1; (b) D_2; (c) D_3; (d) normalized reactive power; (e) normalized current RMS value; (f) objective f.

IV. Simulation and Experimental Analysis

A small DAB dc-dc converter laboratory prototype has been constructed in the laboratory to verify the theoretical analysis. Detailed simulation and experimental results are presented in this section. The experiments are based on low-voltage battery charging. The primary side of the DAB converter is connected to the DC-bus, and the DC voltage is 50V. The secondary side is connected to the battery. The rated voltage of the battery is 12V, and the range of the 1us. The main parameters of the laboratory prototype are listed in Table II, and the maximum rated transmission power of this laboratory prototype is about 130 W.

A. Simulation Results of PSO

Through the PSO simulation of a DAB converter in Matlab/Simulink, when U_2 =12V, P =5W and λ_0 is set to 10000, the evolutionary trajectories of PSOs with different λ are shown in Fig. 8. From Fig. 8, it can be seen that the optimization results are the same when λ<1 and that the reactive power is minimized when the RMS value of the inductor current is minimized. Therefore, in order to minimize these two targets simultaneously and to simplify the objective functions, the RMS value of the inductor current can be used as the objective function of optimization. For other power levels, this conclusion can also be obtained by simulation.

When U_2=12 V, the evolutionary trajectories of PSOs with different transmission powers are shown in Fig. 9. The value of D_1 increases as the transmission power increases, and the optimized reactive power is always a constant at different powers. According to the definition of reactive power in (22) and the shadow in Fig. 2, the optimal reactive power reflects the minimum inductor current required to complete the resonant process in Fig. 3(c). From the equivalent circuit of this resonant process in Fig. 4, it can be seen that this minimum inductor current is related to the initial state and the electrical parameters of the circuit and that it is not related to the transmission power. Therefore, for the same converter with the same DC voltage, the theoretical analysis also shows that the optimized reactive power is a constant at different transmission powers. When the power and D_1 are increasing, according to (30), the value of D_2 also increases. When the transmission power is 40W, D_2 is close to 1. Therefore, 40 W is close to the maximum transmission power for optimized operation at a light load. When the value of D_2 gets closer to one, the TPS control becomes more and more similar to the EPS control.

B. Experimental Results

Operating waveforms of the converter at different transmission powers are shown in Fig. 10, when U_2 is maintained at 12V. The purple waveforms represent six times the inductor current. From Fig. 10, while compared to Fig. 2, the transition of the equivalent ac output voltages of two full bridges occurs in a dead-band. The voltage waveforms are very smooth during each transition, and there are no undesirable phenomena as presented in [19]. The direction of the inductor current in Fig. 10 satisfies the soft-switching constraints in each of the dead-bands. These current waveforms show that the converter has the necessary conditions for obtaining soft-switching. The part of the current required for

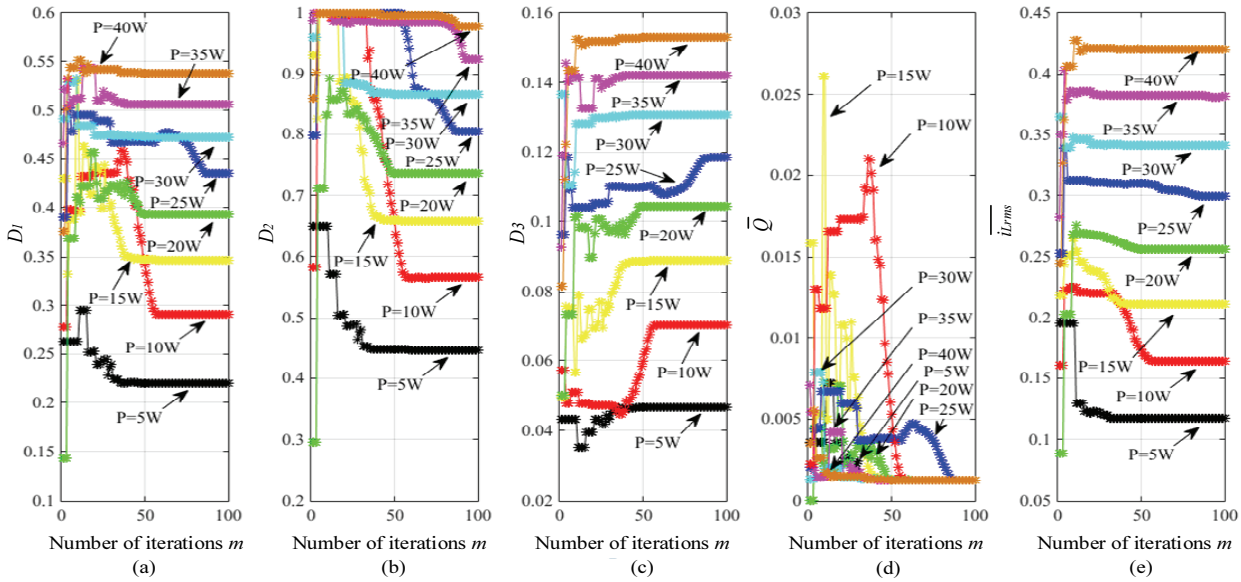

Fig. 9. Evolutionary process and optimal results of PSO at different transmission powers when U_2=12V: (a) duty cycle D_1; (b) duty cycle D_2; (c) duty cycle D_3; (d) normalized reactive power; (e) normalized current RMS value.

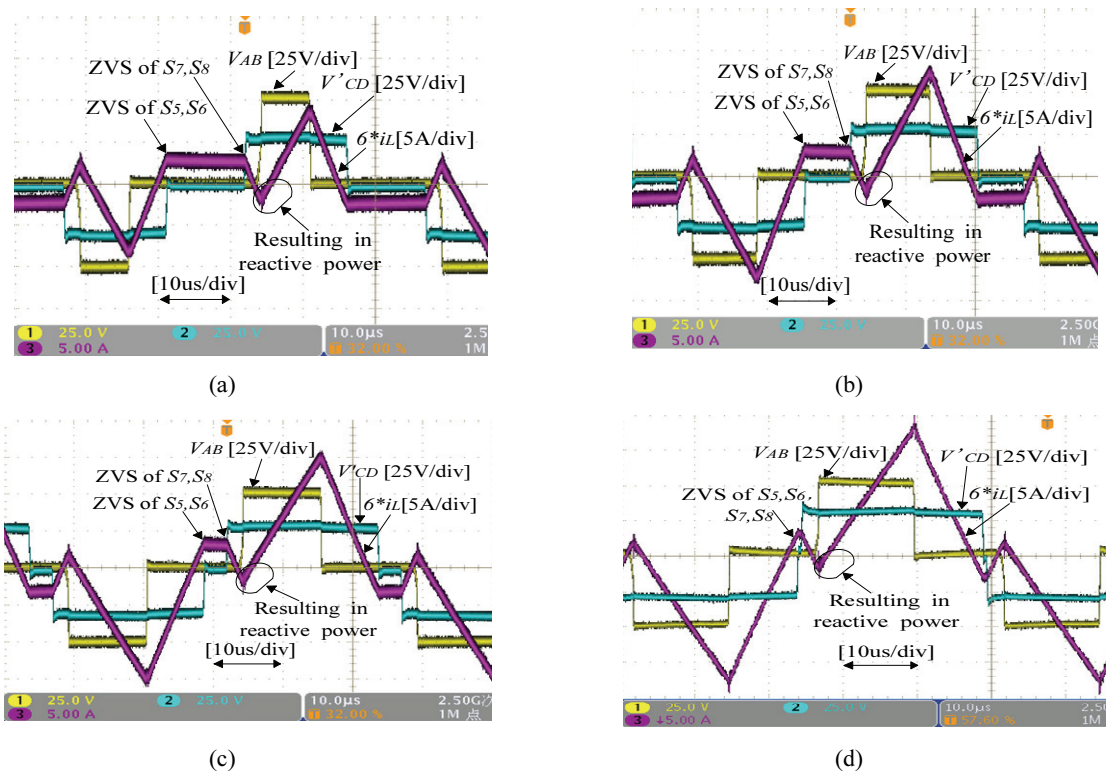

Fig. 10. Operating waveforms at different transmission powers when U_2 = 12 V: (a) P = 10 W; (b) P = 20 W; (c) P = 30 W; (d) P = 40 W.

the ZVS of S_3 and S_4, which causes the reactive power, is basically the same under different transmission power conditions. This is consistent with the simulation results. The inductor current amplitude, which is needed to achieve the soft-switching of S_5, S_6, S_7 and S_8, is also basically the same at different powers. Similarly, the reason for this phenomenon is the same as the same reactive power at different powers. This shows the consistency among theoretical analysis, simulation and experimentation. It also proves that the optimized operation of the converter can accurately control the inductor current. According to current waveform in Fig. 10, the inductor current required to achieve soft-switching produces a small amount of reactive power and increases the RMS value of the current. However, with the power increases, this increment of the RMS value of the current becomes smaller and smaller.

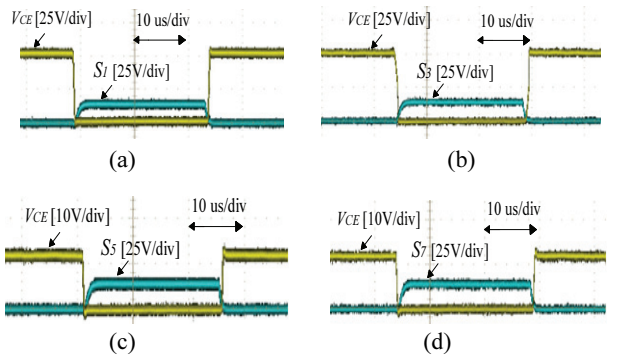

Fig. 11. Operating waveforms of driving signals and switching terminal voltages when U_2 = 12V and P = 10 W: (a) S_1; (b) S_3; (c) S_5; (d) S_7.

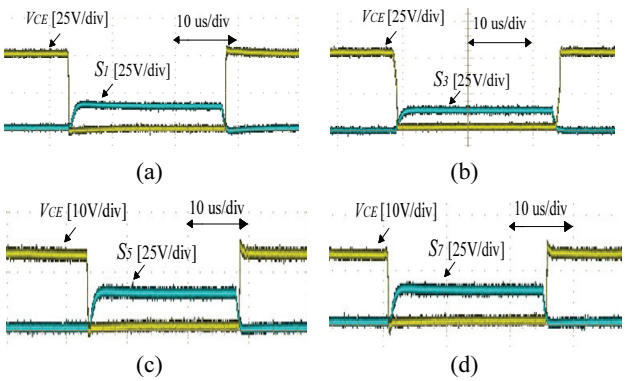

Fig. 12. Operating waveforms of driving signals and switching terminal voltages when U_2 = 12 V and P = 40 W: (a) S_1; (b) S_3; (c) S_5; (d) S_7.

According to an analysis of the soft-switching in section II, all of the switches are turned off with approximate ZVS because the voltage of the parallel capacitor cannot be mutated, and all of the switches are turned on with ZVS because the anti-parallel diode is conducted. Therefore, the ZVS in the turn-off time is not discussed at here. When U_2 =12V, operating waveforms of the driving signal and switching terminal voltage (V_{CE}) at P=5W and P=40W are shown in Fig. 11 and Fig. 12, respectively. It can be clearly seen that the switching terminal voltages have been reduced to zero before the driving signals of S_1, S_5 and S_7 jump from zero to high. The direction of the currents in Fig. 10(a) and 10(d) satisfy the soft-switching constraints in each dead-band. Then, the anti-parallel diode conducts before the switch is turned on. Therefore, the switches S_1, S_2, S_5, S_6, S_7 and S_8 are turned on at full ZVS. From Fig. 11(b) and Fig. 12(b), the terminal voltage of S_3 is reduced to zero at the point where the driving signal starts to rise. This indicates that S_3 and S_4 achieve ZVS at different powers.

This experiment is divided into two parts, one is to compare the different phase-shift controls, while the other is to compare different optimization strategies with the TPS control. Because the operating mode of a light-load with the TPS control is analyzed in this paper, the comparison experiment is only carried out under the light-load condition.

For the EPS control, the selected operating mode satisfies $D_1+2D_3 \le 1$, where D_2 =1. For the DPS control, the selected operating mode satisfies $D_1 \ge D_3$ and $D_1+D_3 \le 1$, where $D_2 = D_1$. Here, the definitions of D_1, D_2 and D_3 are the same as in Fig. 2. In addition, Fig.13 shows efficiency curves of a converter varied with the transmission power in the four phase-shift control when V_2 = 12 V. It can be easily seen that the TPS control with the optimization strategy proposed in this study can achieve a higher efficiency than the other phase-shift controls, particularly in low transmission power conditions. When the power increases, the efficiency is closer in a comparison between the TPS control and the EPS control.

For a comparison of different optimization strategies with the TPS control at a light-load, the analyses in [15] and [16]

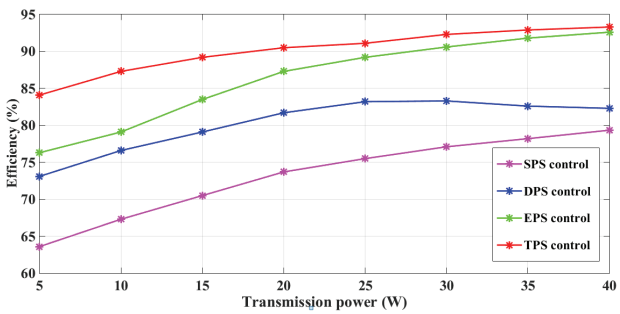

Fig. 13. Efficiency curves varied with the transmission power in different control strategies with U_2 = 12 V.

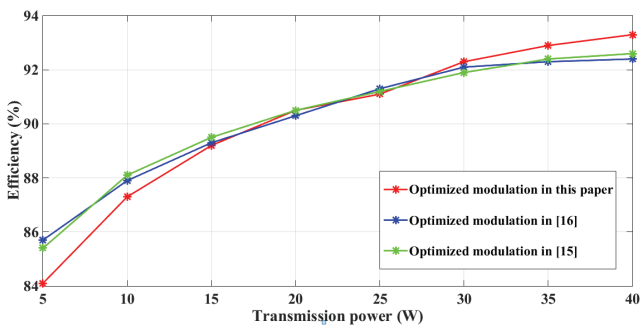

Fig. 14. Efficiency curves varied with the transmission power in different optimized modulation with U_2 = 12 V.

are compared here. In [15] and [16], the soft switching constraints are not directly used as a prerequisite for the optimal operation of the converter. In [15], the current stress is used as the optimization target to determine D_1 and D_3. On this basis, the square of the RMS value of the inductor current is used as the optimization target to determine D_2. In [16], the RMS value of the inductor current as the optimization target to determine the three-degree-of-freedom of the TPS control and the simplified soft-switching constraints are considered here. Efficiency curves of three different optimization strategies are shown in Fig.14. According to the two optimization strategies in [15] and [16], solutions of D_1, D_2, D_3 obtained by these two strategies are similar at a light-load. Thus, the efficiency curves of these two strategies, shown in

Fig. 14, are basically the same. In this paper, the converter is optimized directly in the soft-switching operation area. Therefore, the converter can better realize the soft switch. However, it will produce a small amount of reactive power and increase the RMS value of the current. When the power is low, the reactive power and increment of the RMS value reduce the efficiency of the converter. However, when the power increases, the increment of the RMS value of the current that is caused by the inductor current and required to achieve the soft-switching becomes smaller. Therefore, as shown in Fig.14, when the power is very low, the efficiency of the optimization strategy in this paper is lower than the others. However, with an increase of the power, this efficiency is higher. Therefore, the soft-switching of the converter under light load conditions has its advantages and disadvantages. It reduces the switching losses and improves the switching environment, but adds an amount of reactive power and increases the RMS value of the current. However, with an increase of the power, the disadvantages of soft-switching become smaller and smaller. In this paper, on the basis of soft-switching for all of the switches, the reactive power and the RMS value of the current are minimized simultaneously.

V. CONCLUSIONS

This paper provides an analysis of a DAB with the TPS control at a light-load. The major contributions of this paper include the following. 1) In order to get the exact ZVS constrains, the process of resonance is analyzed in detail in each dead-band. This method of ZVS analysis can be applied to other operating modes. 2) A reasonable dead-band setting method is proposed to satisfy the completion of the resonant process in each dead-band. 3) A constrained optimization problem of the converter is formulated and simulations show that having the RMS value of the current as the objective function can minimize the reactive power. 4) The PSO algorithm is used to analyze and solve this optimization problem. Experimental results show that soft-switching for all of the switches is realized and that the converter works effectively with the proposed strategy.

ACKNOWLEDGMENT

This work was supported by the National Natural Science Foundation of China under Grant No.61622311, No.61573382 and No.61503417, and the Fundamental Research Funds for the Central Universities of Central South University under Grant No.2017zzts494.

REFERENCES

[1] R. W. A. A. De Doncker, D. M. Divan, and M. H. Kheraluwala, "A three-phase soft-switched high-power-density DC/DC converter for high-power applications," *IEEE Trans. Ind. Appl.*, Vol. 27, No. 1, pp. 63-73, Jan./Feb. 1991.

[2] L. Xue, Z. Shen, D. Boroyevich, P. Mattavelli, and D. Diaz, "Dual active bridge-based battery charger for plug-in hybrid electric vehicle with charging current containing low frequency ripple," *IEEE Trans. Power Electron.*, Vol. 30, No. 12, pp. 7299-7307, Dec. 2015.

[3] Y. Shi, R. Li, Y. Xue, and H. Li, "Optimized operation of current-fed dual active bridge DC–DC converter for PV applications," *IEEE Trans. Ind. Electron.*, Vol. 62, No. 11, pp. 6986-6995, Nov. 2015.

[4] H. Zhou, T. Duong, S. T. Sing, and A. M. Khambadkone, "Interleaved bi-directional dual active bridge DC-DC converter for interfacing ultracapacitor in micro-grid application," in *2010 IEEE International Symposium on Industrial Electronics (ISIE)*, pp. 2229-2234, Jul. 2010.

[5] H. J. Chiu and L. W. Lin, "A bidirectional DC-DC converter for fuel cell electric vehicle driving system," *IEEE Trans. Power Electron.*, Vol. 21, No. 4, pp. 950-958, Jul. 2006.

[6] S. P. Engel, M. Stieneker, N. Soltau, S. Rabiee, H. Stagge, and R. W. De Doncker, "Comparison of the modular multilevel DC converter and the dual-active bridge converter for power conversion in HVDC and MVDC grids," *IEEE Trans. Power Electron.*, Vol. 30, No. 1, pp. 124-137, Jan. 2015.

[7] B. Zhao, Q. Yu, and W. Sun, "Extended-phase-shift control of isolated bidirectional DC–DC converter for power distribution in microgrid," IEEE Trans. Power Electron., Vol. 27, No. 11, pp. 4667-4680, Nov. 2012.

[8] M. H. Ryu, H. S. Kim, J. W. Baek, H. G. Kim, and J. H. Jung, "Effective test bed of 380-V DC distribution system using isolated power converters," *IEEE Trans. Ind. Electron.*, Vol. 62, No. 7, pp. 4525-4536, Jul. 2015.

[9] M. N. Kheraluwala, R. W. Gascoigne, D. M. Divan, and E. D. Baumann, "Performance characterization of a high-power dual active bridge DC-to-DC converter," *IEEE Trans. Ind. Appl.*, Vol. 28, No. 6, pp. 1294-1301, Nov./ Dec. 1992.

[10] H. Wen and B. Su, "Reactive power and soft-switching capability analysis of dual-active-bridge DC-DC converters with dual-phase-shift control," *J. Power Electron.*, Vol. 15, No. 1, pp. 18-30, Jan. 2015.

[11] M. Kim, M. Rosekeit, S. K. Sul, and R. W. A. A. De Doncker, "A dual-phase-shift control strategy for dual-active-bridge DC-DC converter in wide voltage range," in *IEEE 8th International Conference on Power Electronics and ECCE Asia (ICPE & ECCE)*, pp. 364-371, Jun. 2011.

[12] K. Wu, C. W. de Silva, and W. G. Dunford, "Stability analysis of isolated bidirectional dual active full-bridge DC–DC converter with triple phase-shift control," *IEEE Trans. Power Electron.*, Vol. 27, No. 4, pp. 2007-2017, Apr. 2012.

[13] F. Krismer and J. W. Kolar, "Closed form solution for minimum conduction loss modulation of DAB converters," *IEEE Trans. Power Electron.*, Vol. 27, No. 1, pp. 174-188, Jan. 2012.

[14] N. Hou, W. Song, and M. Wu, "Minimum-current-stress scheme of dual active bridge DC–DC converter with unified-phase-shift control," *IEEE Trans. Power Electron.*, Vol. 31, No. 12, pp. 8552-8561, Dec. 2016.

[15] J. Huang, Y. Wang, Z. Li, and W. Lei, "Unified triple-phase-shift control to minimize current stress and achieve full soft-switching of isolated bidirectional DC–DC

converter," *IEEE Trans. Ind. Electron.*, Vol. 63, No. 7, pp. 4169-4179, Jul. 2016.

[16] M. Yang, *PWM plus phase-shift control for dual active full-bridge DC-DC converter*, M.S. thesis, Dept. Electrical. Eng., Nanjing Univ. of Aeronautics and Astronautics., Nanjing, China, 2013.

[17] H. Bai and C. Mi, "Eliminate reactive power and increase system efficiency of dual active bridge DC–DC converters using novel dual-phase-shift control," *IEEE Trans. Power Electron.*, Vol. 23, No. 6, pp. 2905-2914, Nov. 2008.

[18] B. Zhao, Q. Song, and W. Liu, "Efficiency characterization and optimization of isolated bidirectional DC–DC converter based on dual-phase-shift control for DC distribution application," *IEEE Trans. Power Electron.*, Vol. 28, No. 4, pp. 1711-1727, Apr. 2013.

[19] B. Zhao, Q. Song, W. Liu, and Y. Sun, "Dead-time effect of the high-frequency isolated bidirectional full-bridge DC–DC converter: comprehensive theoretical analysis and experimental verification," *IEEE Trans. Power Electron.*, Vol. 29, No. 4, pp. 1667-1680, Apr. 2014.

[20] J. Li, Z. Chen, Z. Shen, P. Mattavelli, J. Liu, and D. Boroyevich, "An adaptive dead-time control scheme for high-switching-frequency dual active bridge converter," in *Twenty-Seventh Annual IEEE Applied Power Electronics Conference and Exposition (APEC)*, pp. 1355-1361, Feb. 2012.

[21] J. Riedel, D. G. Holmes, C. Teixeira, and B. P. McGrath, "Harmonic-based determination of soft-switching boundaries for 3-level modulated single-phase dual active bridge converters," in *IEEE Energy Conversion Congress and Exposition (ECCE)*, pp. 1505-1512, Sep. 2015.

[22] M. Ryu, D. Jung, J. Baek, and H. Kim, "An optimized design of bi-directional dual active bridge converter for low voltage battery charger," in *16th International Power Electronics and Motion Control Conference and Exposition (PEMC)*, pp. 177-183, Sep. 2014.

[23] Y. Shi and R. Eberhart, "A modified particle swarm optimizer," in *IEEE International Conference on Evolutionary Computation Proceedings, IEEE World Congress on Computational Intelligence.*, pp. 69-73, May 1998.

[24] A. Ratnaweera, S. K. Halgamuge, and H. C. Watson, "Self-organizing hierarchical particle swarm optimizer with time-varying acceleration coefficients," *IEEE Trans. Evol. Comput.*, Vol. 8, No. 3, pp. 240-255, Jun. 2004.

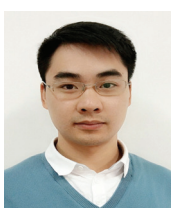

Li Jiang was born in Hunan, China, in 1991. He received his B.S. degree in Automation from the Hunan University of Technology, Zhuzhou, China, in 2015. He is presently working towards his M.S. degree in Control Science and Engineering in the School of Information Science and Engineering, Central South University, Changsha, China. His current research interests include bidirectional DC/DC converters and solid-state transformers.

Yao Sun was born in Hunan, China, in 1981. He received his B.S., M.S. and Ph.D. degrees from the School of Information Science and Engineering, Central South University, Changsha, China, in 2004, 2007 and 2010, respectively. He is presently working as a Professor in the School of Information Science and Engineering, Central South University. His current research interests include matrix converters, microgrids and wind energy conversion systems.

Mei Su was born in Hunan, China, in 1967. She received her B.S. and M.S. degrees in Industrial Automation, and her Ph.D. degree in Control Science and Engineering from the School of Information Science and Engineering, Central South University, Changsha, China, in 1989, 1992 and 2005, respectively. Since 2006, she has been working as a Professor in the School of Information Science and Engineering, Central South University. Her current research interests include matrix converters, adjustable speed drives and wind energy conversion systems.

Hui Wang was born in Hunan, China, in 1984. He received his B.S., M.S. and Ph.D. degrees from the School of Information Science and Engineering, Central South University, Changsha, China, in 2008, 2011 and 2014, respectively. Since 2016, he has been working as a Lecturer in the School of Information Science and Engineering, Central South University. His current research interests include matrix converters, DC/DC converters and solid-state transformers.

Hanbing Dan was born in Hubei, China, in 1991. He received his B.S. degree in Automation from Central South University, Changsha, China, in 2012, where he is presently working towards his Ph.D. degree in Electrical Engineering. He was a Visiting Researcher in the Faculty of Engineering at the University of Nottingham, Nottingham, ENG, UK, from November 2016 to November 2017. His current research interests include AC/DC converters, matrix converters, finite control set-model predictive control, fault diagnosis and fault tolerance of power electronics, and wireless power transmission.